Accuracy of rapid prototype models for head and neck reconstruction

Robert M Taft, DDS,[a] Shayne Kondor, MSAE,[b] and Gerald T. Grant DMD, MS[c]
Naval Postgraduate Dental School, Bethesda, Md

Statement of problem. Rapid prototype (RP) models are used in craniofacial reconstructions; however, there are no standards or acceptable limits to ensure accuracy of the fabricated models.

Purpose. The purpose of this study was to assess the accuracy of RP models by validating the accuracy of SLA skull models with a coordinate measurement device.

Material and methods. Stainless steel spheres were located on a dry cadaver skull as fiducial markers, scanned with Multi Detector Computer Tomography (MDCT), and interpreted with software for rapid prototyping. Seven stereolithographic (SLA) models were fabricated and measured with a coordinate measurement device. An Euler rotation transformation calculation was applied to standardize the coordinate system between the control and the models. A paired standard *t* test (α=.05) was used to compare fiducial marker locations on SLA models with the control.

Results. A significant difference was found between the control and each of the SLA models (P<.001) in the Z axis additive build. Significant dimensional differences were not consistently detected in the X and Y axes. Dimensional deviations fell within the size of the MDCT scans voxel dimensions.

Conclusions. The greatest discrepancies of medical model fabrication correspond to the largest dimension of the orthotropic voxel volume of the MDCT scan, which is related to the slice thickness of the scan and the Z axis of the RP model. However, the absolute magnitude of the error was small, well within the generally accepted tolerance for patient treatment. (J Prosthet Dent 2011;106:399-408)

Clinical Implications

As emerging technology, many of the processes used to enlist digital planning and additive manufacturing for reconstruction and implant treatment are based on the assumption that the computer manufactured product is as accurate as the digitally created plan. It is imperative understand and be sure of the accuracy of the systems to provide products such as cutting guides and positioning guides for surgical reconstruction, and drill guides for dental implant placement.

Disclaimer:
The views expressed in this article are those of the authors and do not necessarily reflect the official policy, position, or endorsement of the Department of the Navy, Army, Department of Defense, nor the U.S. Government. We certify that all individuals who qualify as authors have been listed; each has participated in the conception and design of this work, the analysis of data, the writing of the document, and the approval of the submission of this version; that the document represents valid work; that if we used information derived from another source, we obtained all necessary approvals to use it and made appropriate acknowledgements in the document; and that each takes public responsibility for it. Authors acknowledge that research protocol MPTE2010.002 Accuracy of Rapid Prototype Models for Head and Neck Reconstruction received applicable NNMC Institutional Review Board review and approval.

[a]Captain, Dental Corps, United States Navy; Dean.
[b]Chief Engineer, Craniofacial Imaging Research.
[c]Captain, Dental Corps, United States Navy; Director, Craniofacial Imaging Research.

Computer-aided design (CAD) and computer-aided manufacturing (CAM) techniques have facilitated the design and rapid production of mass numbers of accurate parts by the manufacturing industry in a timely manner. Additive layered fabrication CAM processes introduced the ability to produce unique parts with similar accuracy and speed. Rapid Prototyping (RP) is the production of unique parts directly from digital CAD data. Manufacturing unique items by RP techniques has many applications in dentistry and medicine.

In the adaptation of CAD/CAM for dental or medical use, a scanned Digital Imaging and Communication in Medicine (DICOM) file is converted to a CAM-friendly file format. Modeling from DICOM requires manipulation of images to account for dimension, source, and artifacts that are common in dental/medical scanning but not found in the direct CAD designed processes.

Conventional computed tomography (CT) and cone beam CT images are used with CAD software to generate highly accurate virtual models of patient-specific anatomy. Combined with rapid prototyping (RP) techniques, such as 3-dimensional (3-D) printing and stereolithography (SLA), these virtual models are transformed into tangible 3-D models and have been found useful for planning and fabricating surgical templates and custom implants for craniofacial reconstruction. When compared to the original structures, the accuracy of these models is reported to be within the limits for treatment planning and the fabrication of custom methylmethacrylate cranial implants.[1,2] In the absence of pretraumatic craniofacial records, medical modelers must resort to virtual mirroring of the contralateral, intact anatomy with software and then modify the model to fit the size and contour of the craniofacial defect by using cut and paste methods.[3,4] As a result, advanced digital imaging in dentistry and medicine has given rise to a range of software developed for surgical reconstructive/rehabilitative solutions. These solutions are either associated with the RP fabrication of surgical guides and custom implants or used to program navigational systems to guide implant placement and maxillofacial reconstructions.[5] Although this technology has greatly advanced, care must be taken to ensure that the human anatomy generated by imaging, digital manipulation, and ultimately a medical rapid prototyped product is subject to rigorous quality assurances.[4]

The accuracy of an RP model is determined by stacking tolerances in the CT scanning, CAD modeling and the RP fabrication processes. Previous studies of RP anatomic model accuracy have measured the positions of landmarks on a CT image of a phantom in software and then compared these measurements to the physical locations on the RP model on the basis of linear measurement with calipers.[6-7] These types of studies are affected by the observer's choice of where to measure the anatomical landmarks on the CT image in relation to the RP model. Recent studies have used radiopaque markers (fiduciary points) placed at multiple locations on a skull phantom; these landmarks, reproduced on the resulting models, were measured against the radiographic representation from point to point.[8,9] However, caliper measurements can be subjective in that they are affected by the positioning of the caliper on both the RP models and controls (phantom).[10] Therefore, a repeatable, observer-independent method to compare the control's dimensions to the resulting model's dimensions is necessary to assess model accuracy in reproducing the original anatomy.

Geometric dimensioning and tolerancing (GD&T) techniques are used in the manufacturing industry for quality control of precision parts.[11] Well designed feature measurements clearly communicate a 3-D geometry in the language of GD&T. Specific features, such as centroids of spheres or centerlines of holes, are referenced to a common datum (origin) to describe a part; these feature locations are determined from the measurements of discrete points from which the feature location is computed. Point-to-point coordinate measurement devices (CMD) can locate a given point in Euclidean space (with reference to orthogonal x, y, and z coordinate axes) and relate it to a common datum with submillimeter precision. This precision part inspection approach appears ideal to assess the accuracy of RP models against the original scanned source and could be used as the standard for quality assurance of model accuracy. This paper seeks to validate this concept by comparing the means of a control anatomic model with fiducial markers with the manufactured model by using a contact measurement device and testing the null hypothesis that the means of the fiducial marker locations measured on the models and control do not differ.

MATERIAL AND METHODS

Control Model

An overview of the procedures followed in this study is presented in Figure 1. An edentulous dry human skull without the mandible and with a sectioned calvarium retained with metal pins and clasps was selected for the control and prepared for CT scanning by removing the metal hardware. The calvarium was affixed with a bead of alpha-cyanoacrylate ester (CA) adhesive (Permabond 910; Permabond Engineering Adhesives, Pottstown, Pa). After the adhesive polymerized, the calvarium was gently pried free, leaving a circumferential indexing groove for repeatable realignment. Eight stainless steel spheres, 5.00 ± 0.005 mm in diameter, were attached to the skull as fiduciary markers with CA adhesive. Markers were distributed over the skull surface at 7 locations (vertex, nasion, occipital, mastoid (bilateral) and temporal (bilateral) typically involved in craniofacial reconstruc-

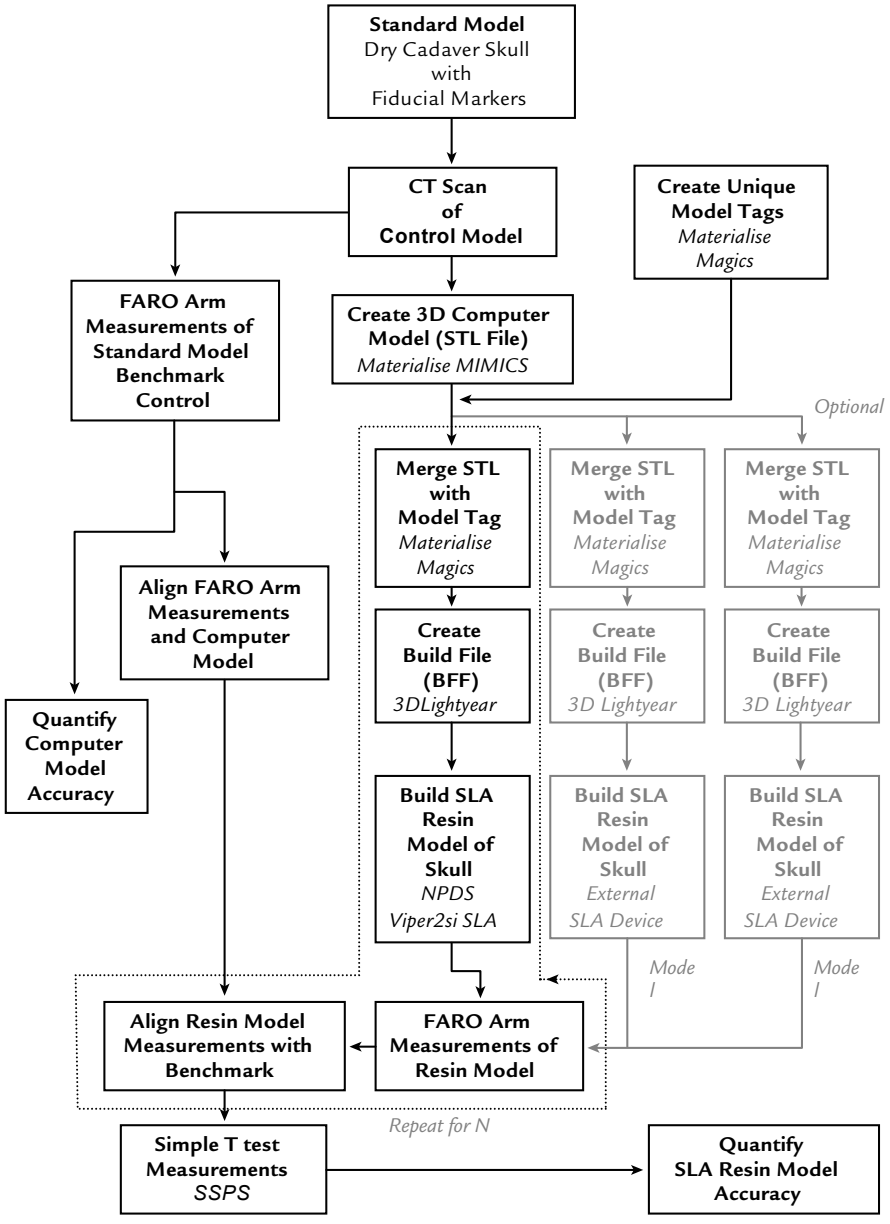

1 Experimental design.

tion.[12] The calvarium was removed and a marker was positioned at the Sella turcica; this marker served as a reference location for all measurements.

Benchmark Measurements of the Control Model

The volumetric center (centroid) of each fiducial marker was accurately located with a coordinate measurement device (FARO Gage; FARO Technologies Inc, Lake Mary, Fla) with a 3 mm ball tip probe. The FARO Gage CMD is purported by the manufacturer to be a precise CMD with accuracy certified per ISO 10360-2 with a resolution of 0.1 mm along all axes accuracy of ± (5+8L/1000) mm on all axes over a 1200 mm working span (L), and a probing error of 0.006 mm, measuring the diameter of a 25.4 mm sphere. The accuracy of this CMD is at least one order of magnitude greater than the finest resolution of the SLA device; thus, it was deemed a suitable device to obtain benchmark locations of the fiduciary markers on the standard model.

The CMD and the control were affixed to a 100 mm thick granite surface table (FARO Technologies Inc) to be measured. The CMD was mounted to the factory installed threaded base on the surface of the granite table, and the control was affixed to the table with a custom mounting platform fabricated from epoxy resin. To prevent stresses on the control, the platform was first clamped to the granite table and then the control was affixed to the platform with CA adhesive (Fig. 2). Point location measurements were made by touching the ball probe to the point of interest at an arbitrary angle; the exact point of probe contact was computed from the articulation angles of the CMD arm.

Point measurements were used to construct a reference datum, define a common origin, and determine the centroid location of each fiduciary marker. The reference X-Y datum plane was established by sampling a minimum of 3 points on the granite surface table, followed by 1 above the table to establish the +Z direction. The +X axis was defined by sampling a minimum of 2 points, from left to right, along the line of contact between the mounting platform and the granite table. The +Y axis was implicitly defined in a right-hand Cartesian coordinate system. The calvarium was temporarily removed to access the Sella turcica, in the central cranial fossae. The centroid of the spherical fiducial marker at the Sella turcica, was determined to define an origin point for the coordinate axes. Points were measured at the top-center of the sphere and at 4 evenly spaced locations on the equator as shown in Figure 3. The sphere's centroid location (relative to the base of the CMD) was calculated in software (FARO 1.5 software) by fitting a sphere to the sampled points and determining the location of its geometric center. If the diameter of the fitted sphere matched the known diameter of the fiducial marker within the accuracy of the measurement device, the measurement was accepted; otherwise it was repeated. The centroid of the sphere at the Sella turcica, was assigned as

2 Control model mounted for measurement.

3 Measurement of sella turcica, fiducial marker position on control using 3 mm contact probe.

the common origin point of the measurement coordinate system.

The locations of the 7 surface fiducial marker centroids were measured with reference to the common origin. The calvarium was repositioned and secured in place with CA adhesive. The position of each surface fiducial marker was measured by using the same protocol as for the marker at the Sella turcica. The 3-D position of each sphere's centroid was automatically calculated by the software (FARO 1.5). The diameter of the fitted sphere and the maximum deviation between the individual point measurements and the sphere surface, a quantity called *form* in the software's data output, were used as acceptance criteria for fiducial marker measurements. Acceptable measurements on the control were specified to be within ± 0.005 μm for both the fitted sphere diameter and reported form.

The measurement process was scripted in the software application, allowing for repeatable application of the measurement process. The script included the initial measurements necessary to establish the reference coordinate system and the fiducial marker (centroid) positions. The control was measured 5 times, following the scripted process. In each measurement set, the fiducial marker diameters (sphere fits) were within the range 5.000 ± 0.005 mm; thus, the spheres were consistently measured at their known diameter within the accuracy of the CMD. Similarly, the reported form fell within the same range; thus, this small sample size was deemed acceptable because of the small observed variation among the independent measurements. By using these 5 measurements, a mean centroid location was calculated for each fiducial marker to establish the benchmark (standard qualification) positions on the control. Measurements on the rapid prototyping models were compared to this benchmark.

Computer Model of the Control

A computer model of the control was obtained by CT scanning the skull with markers and then reconstructing the tomographic data as a 3-D volumetric model. The control was positioned to simulate a supine patient and scanned on a CT scanner (Phillips Brilliance 40 Multi Detector CT Scanner; Philips Healthcare, Andover, Mass) at the National Naval Medical Center Department of Radiology, Bethesda, Md. The scan was sampled axially, along a line between the Sella turcica, and bregma. Tomographic images were reconstructed at the scanner workstation. Slice images were generated at a 0.625 mm slice interval with a 0.42 mm pixel resolution in the plane of the slice. Radiodensity values, Hounsfield Units (HU), were encoded as grayscale values assigned to the pixels; zero radiodensity was represented as black, maximum radiopacity as white, and all values in between as shades of gray; all were encoded with 12 bit resolution (4096 shade steps). The image set was exported in DICOM 3.0 format.

The DICOM dataset was imported into the medical image viewing and modeling software (MIMICS 12.1; Materialise Dental, Plymouth, Mich), where the tomographic data was reconstructed as a volumetric (3-D) digital model. Image slices were segmented into pixel datasets based on thresholding grayscale values. Contiguous sets of pixels in the stack of slice images were further grouped into individual pixel subsets or masks, representing the bone and metal fiducial makers. Where necessary, metal artifact streaks in the mask were manually deleted, taking care not to affect the image of the fiducial markers. Volumetric (3-D) digital models were computed by interpolating surfaces with utilities in the software. The volumetric models of bone and fiducial markers were joined into a single model by a Boolean operation. Finally, the model was exported into the STL file format, a discrete surface/volume representation consisting of triangular facets connected at corner nodes; it is the standard format used for rapid prototyping.

The STL model was prepared for fabrication with rapid prototyping

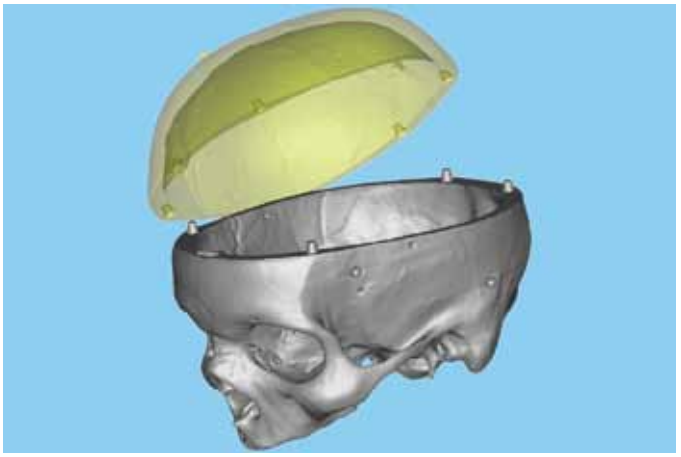

4 Digital model of skull with conical alignment features added to calvarium and base.

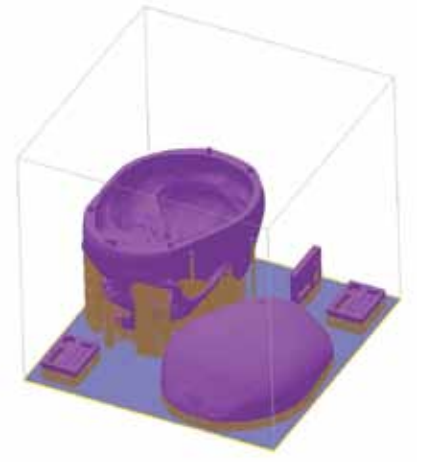

5 Model of skull arranged for fabrication on SLA; model parts are shown in purple, added support structure in tan.

Table I. Build chamber temperature, humidity, and SLA resin viscosity remained within manufacturer's specified operating limits during fabrication of each model

	Observed High	Observed Low	Ideal
Build chamber temperature	23.9°C	22.8°C	≤28°C
Build chamber humidity	37%	30%	0 % - 50%
SLA Resin vat temperature	29.9°C	27.8°C	28°C
SLA Resin viscosity*	16.0 sec	16.5 sec	14 to 19 sec

software (Magics 13.0; Materialise Dental). Minor inconsistencies in the surface of the 3-D volume, such as inverted facets or small holes, were detected and fixed. The digital model was split along the existing calvarium separation line on the control to allow access to the fiducial marker in the central cranial fossae. Indexing features were added to both digital models to allow the assembly of the halves of the rapid prototype (RP) models. The calvarium and cranial base were stored as individual STL files. The STL file set of the control was the common definition used to produce all RP replicas of the control. A rendering of the STL model is shown in Figure 4.

Rapid Prototyping Fabrication of the Skull Models

Seven RP models were fabricated on an SLA device (Viper2Si SLA; 3D Systems, Rock Hill, SC). The SLA RP models were tangible, 3-D polymer replicas of the control, generated layer-by-layer by selective photo-polymerization of a liquid monomer epoxy resin (Accura 60 SLA epoxy resin; 3D Systems, Rock Hill, SC). The epoxy resin produced transparent models with properties similar to polycarbonate.

Unique identification tags were fabricated with each SLA model. Each tag was a prismatic block embossed with the model number and fabrication date. Regular geometric features with precisely known dimensions were incorporated into the tags for quality control evaluations on each SLA build.

Machine control code for the SLA was generated from the STL models of the control and the identification tags. Build design and control code generation were performed with 3-D software (3D Lightyear 1.5.2; 3D Systems Corp, Rock Hill, SC). The STL models of the cranial base and calvarium, along with 3 identical identification tags, were positioned within the SLA machine's build volume. Support structures necessary to affix the parts in the build volume were added with the automated support function (Fig. 5). Calibration parameters for the SLA machine and choice of resin were applied, and a machine control code for the SLA machine was generated.

All SLA models were fabricated under controlled conditions, built separately, and sequentially named C1 to C7 (on the model identification tags). Upon completion of each SLA build, the parts were promptly cleaned and postpolymerized. Observations of the environmental variables affecting the SLA process, including the build chamber and epoxy resin conditions, were recorded and tracked. All observations of build chamber temperature, humidity, and resin viscosity remained within the manufacturer's specified operating limits during fabrication of each model (Table I). Quality control measurements of geometric features on the model tags were made with a hand caliper; all quality control measurements were considered acceptable, and all models were accepted for evaluation.

Measurement of RP Skull Models

The positions of the fiducial marker centroids, as reproduced on the SLA models, were measured with the CMD and followed the procedure described for measuring the fiducial markers on the control skull. Five independent measurement sets were obtained by using the identical sampling procedure as used on the control. To avoid a bias in the measured centroid position, resulting from fitting spheres to a spherical SLA replication of the fiducial markers, additional measurement sets were made by sampling 10 distributed points on the surface of each fiducial marker. A minimum of 8 independent sets of CMD measurements were recorded and averaged to establish a true centroid position for each fiducial marker on the SLA models.

To account for differences in mounting the SLA models and the control on the surface table, measurements of the SLA model were mathematically corrected to match the control's position relative to the CMD. The centroid of the Sella turcica, was defined as the point of origin for all SLA model measurements conducted with the CMD; all SLA and control measurements were assumed to align on the origin and thus,

TABLE II. Fiducial marker measurements in transformed coordinates

	Landmarks (mm)						
Sample	**L Asterion**	**L Pterion**	**Nasion**	**R Pterion**	**R Asterion**	**Bregma**	**Lambda**
C1'							
X	64.813	55.137	0.410	-61.502	-68.706	-4.013	-7.261
Y	51.513	-17.824	-76.500	-14.798	47.015	0.252	102.767
Z	8.791	39.321	5.487	22.167	-14.576	105.560	57.758
C2'							
X	64.834	55.091	0.432	-61.487	-68.738	-4.014	-7.247
Y	51.557	-17.840	-76.420	-14.833	47.074	0.263	102.770
Z	8.892	39.313	5.548	22.196	-14.510	105.571	57.725
C3'							
X	64.831	55.063	0.423	-61.503	-68.749	-3.997	-7.254
Y	51.507	-17.843	-76.440	-14.861	47.048	0.264	102.786
Z	8.873	39.309	5.537	22.210	-14.546	105.556	57.745
C4'							
X	64.831	55.048	0.365	-61.418	-68.836	-4.022	-7.248
Y	51.546	-17.799	-76.450	-14.844	47.109	0.273	102.742
Z	8.866	39.460	5.534	22.087	-14.315	105.610	57.648
C5'							
X	64.845	55.019	0.423	-61.412	-68.854	-4.040	-7.208
Y	51.542	-17.785	-76.400	-14.902	47.167	0.283	102.746
Z	8.904	39.388	5.619	22.003	-14.263	105.656	57.643
C6'							
X	64.898	55.145	0.369	-61.470	-68.641	-3.966	-7.358
Y	51.517	-17.837	-76.420	-14.824	47.027	0.233	102.815
Z	8.735	39.256	5.428	22.134	-14.654	105.588	57.761
C7'							
X	64.810	55.069	0.468	-61.604	-68.674	-3.966	-7.258
Y	51.483	-17.867	-76.420	-14.883	47.023	0.259	102.815
Z	8.814	39.243	5.517	22.146	-14.600	105.584	57.764
Control							
X	65.037	55.018	0.439	-61.317	-68.749	-3.998	-7.326
Y	51.306	-17.731	-76.730	-14.875	46.964	0.279	102.725
Z	8.410	38.845	4.916	21.750	-14.948	105.949	57.550

Table III. RP model measurement deviation from control

Sample	Landmarks (mm)						
	L Asterion	L Pterion	Nasion	R Pterion	R Asterion	Bregma	Lambda
C1'							
$\|\Delta X\|$	0.224	0.119	0.029	0.184	0.043	0.015	0.065
$\|\Delta Y\|$	0.207	0.093	0.234	0.076	0.051	0.027	0.042
$\|\Delta Z\|$	0.381	0.475	0.571	0.417	0.371	0.389	0.208
C2'							
$\|\Delta X\|$	0.202	0.073	0.007	0.170	0.012	0.016	0.079
$\|\Delta Y\|$	0.251	0.109	0.314	0.042	0.109	0.015	0.045
$\|\Delta Z\|$	0.4	0.468	0.632	0.446	0.438	0.377	0.175
C3'							
$\|\Delta X\|$	0.206	0.045	0.016	0.186	0.001	0.001	0.072
$\|\Delta Y\|$	0.201	0.112	0.292	0.014	0.083	0.015	0.061
$\|\Delta Z\|$	0.463	0.464	0.622	0.461	0.402	0.392	0.195
C4'							
$\|\Delta X\|$	0.205	0.029	0.074	0.101	0.087	0.023	0.078
$\|\Delta Y\|$	0.240	0.068	0.284	0.031	0.145	0.006	0.017
$\|\Delta Z\|$	0.455	0.615	0.618	0.337	0.632	0.338	0.098
C5'							
$\|\Delta X\|$	0.191	0.001	0.016	0.095	0.105	0.042	0.118
$\|\Delta Y\|$	0.236	0.054	0.331	0.027	0.203	0.004	0.021
$\|\Delta Z\|$	0.493	0.543	0.703	0.253	0.684	0.292	0.093
C6'							
$\|\Delta X\|$	0.139	0.126	0.070	0.153	0.108	0.032	0.032
$\|\Delta Y\|$	0.211	0.106	0.317	0.051	0.063	0.046	0.090
$\|\Delta Z\|$	0.325	0.411	0.512	0.384	0.294	0.361	0.211
C7'							
$\|\Delta X\|$	0.226	0.051	0.030	0.287	0.076	0.032	0.068
$\|\Delta Y\|$	0.177	0.136	0.310	0.008	0.059	0.020	0.090
$\|\Delta Z\|$	0.404	0.398	0.601	0.396	0.348	0.365	0.213

only a mathematical rotation was necessary to account for position errors. For each model, a unique Euler rotational transformation was computed by a least squares approach. The Euler rotational transformation aligned the positions of like fiducial markers on the SLA models with the control. The alignment of the measurements and computation of the absolute deviations between each SLA model and the control were computed in a spreadsheet (Microsoft Excel 2003; Microsoft Corporation, Redmond, Wash).

The measured positions of the 7 surface fiducial markers on each of the SLA RP models were compared to corresponding fiducial marker positions on the control. A paired *t* test (α=.05) was performed by using statistical analysis software (SPSS 16; SPSS Inc, Chicago, Ill) to compare the means of the X, Y, and Z coordinates of the fiducial markers.

RESULTS

All comparisons between the RP models and the control were performed in the common coordinate base of the control model. All measurement were determined in a right hand coordinate system with the XY plane aligned closely to the axial slice plane of the CT scan with the build plane of the SLA machine, the X axis running posterior to anterior, and the Y axis medial-lateral positive to the left side of the skull. The Z axis was aligned with the axial direction of the CT scan, and the layer build-up direction of the SLA device positive in the inferior to superior direction. The origin was at the center of the Sella turcica. Measured positions of the fiducial marker centroids, corrected to match this coordinate basis, are provided in Table II. Differences between the control and SLA models are presented in Table III

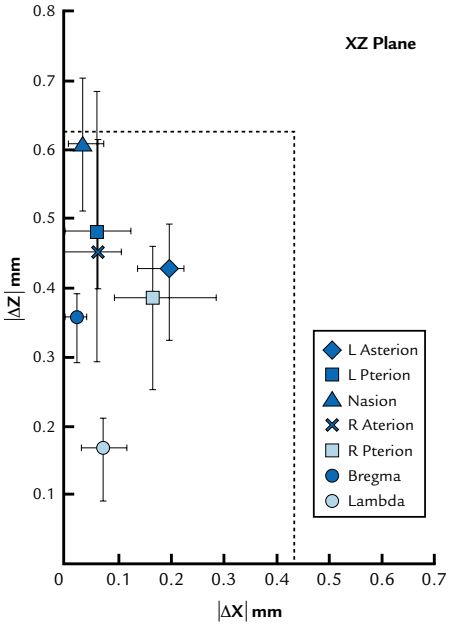

6 Deviations of RP models from control, projected in XZ plane; points denote mean deviation for fiducial marker location, error bars denote extent of deviations; bounding box shows relative size of voxel in CT scan.

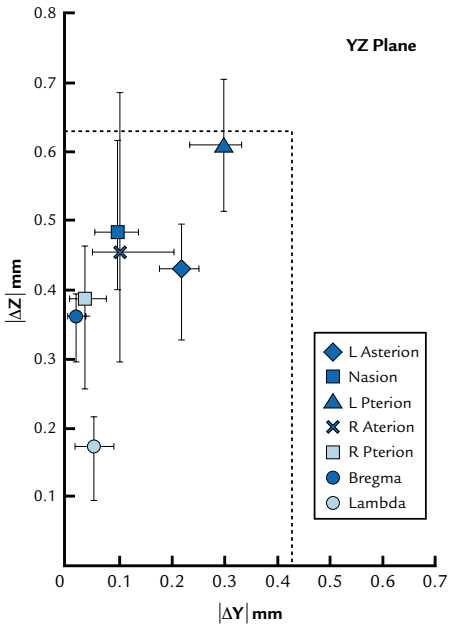

7 Deviations of RP Model from Control in 3-D Space; points denote mean deviation for fiducial marker location, error bars denote extent of deviations; bounding box shows relative size of voxel in CT scan.

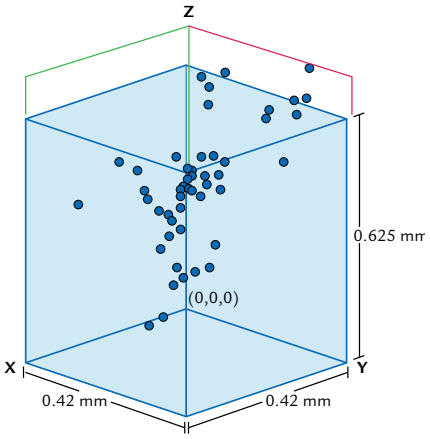

8 Deviations of RP model from control in 3-D Space; bounding box shows relative size of voxel in CT scan.

as absolute values (DX, DY, DZ). The maximum measured error between the control and SLA models occurred at the nasion, with a maximum mean absolute difference of 0.608 (± 0.096) mm Z-axis. Absolute deviations between the SLA models and control ranged from 0.001 mm to 0.703 mm, depending on axis and fiducial marker location; standard deviation ranged from 0.02 mm to 0.23 mm. Mean absolute differences between the fiducial marker locations on the SLA models and control are illustrated in Figures 6 and 7. A scatter plot of all data points in comparison to the MDCT scan voxel volume is presented in Figure 8.

However, the results of the paired *t* test (Table IV) suggest that there were statistically significant differences in most fiducial marker positions on SLA models as compared to the control. Significant differences were observed for 4 of the 7 fiducial markers along the X-axis ($P \leq .01$), 4 of the 7 markers along the Y-axis ($P \leq .01$), and all 7 of the fiducial markers along the Z-axis ($P \leq .001$) (Table IV).

DISCUSSION

The results of the paired *t* test (Table IV) suggest that there was a significant difference in most of the dimensions between the control and the RP models ($P \leq .05$) with a standard deviation of about 0.05 mm, which supports rejecting the null hypothesis. As the use of digital imaging and rapid prototype techniques to assist in treatment planning and treatment for reconstruction becomes more acceptable, it is imperative that there is a method to ensure that the images and the resultant digitally produced model or device are accurate. In addition, the ability to calculate the difference of the point of measurement to a control within an acceptable standard is a desired feature and should be incorporated into the fabrication and quality assurance of the production of medical devices and models. CMD was found to have the sensitivity to detect measurement between the control and the RP models, it was relatively easy to use with learning to manipulate the articulated arm being the most difficult maneuver. Once the software had been programmed to identify the markers, it was simply a matter of following the instructions on the screen from one marker to another. The statistical analysis indicated a significant difference between the SLA models and the control at $\alpha < .05$, specifically along the Z axis, for all fiduciary markers ($P \leq .01$). In contrast, there was no significant difference along the X axis for the nasion, R asterioin, bregma judicial markers or along the Y axis of the R pterion, bregma, and lambda (Table IV).

The axial slice distance of the MDCT scan defines the resolution of the 3-D reconstruction of the digital volumetric model; this axial direction corresponds to the Z axis of the measurement sets. Likewise, the vertical build layer thickness of the SLA process defines the resolution of the SLA RP model. The Z axis is generally the least accurate for geometric replication in the SLA process. Furthermore, quantization errors in processing the

Table IV. Paired *t* test results

Dimension		Mean (mm)	Std Deviation (mm)	*P*
L Asterion				
	X	64.84	0.03	≤.001
	Y	51.52	0.03	≤.001
	Z	8.83	0.07	≤.001
L Pterion				
	X	55.08	0.05	.01
	Y	17.83	0.03	≤.001
	Z	39.33	0.08	≤.001
Nasion				
	X	0.42	0.04	.16
	Y	76.44	0.03	≤.001
	Z	5.52	0.06	≤.001
R Pterion				≤.001
	X	61.48	0.06	
	Y	14.85	0.03	0.14
	Z	22.14	0.07	≤.001
R Asterion				
	X	68.74	0.08	.82
	Y	47.07	0.06	≤.001
	Z	14.5	0.15	≤.001
Bregma				
	X	4	0.03	.78
	Y	0.26	0.02	.1
	Z	105.59	0.04	≤.001
Lambda				
	X	7.26	0.05	.01
	Y	102.7	0.23	.36
	Z	57.72	0.05	≤.001

Sensitivity *P*≤.05

STL computer model into discrete slices for SLA fabrication contribute to overall Z axis error. Therefore, a greater error in replication along the Z axis can generally be expected in the production of RP models.

The MDCT scan resolution is highest in the plane of the axial slice image. The SLA device is most accurate in that plane of the build layer; therefore, smaller deviations can be expected along the X and Y component directions. This is illustrated by the data in Figures 5-7; deviations in the X and Y component directions are generally smaller than in the Z direction.

The maximum deviations from the control were noted at the nasion and L pterion fiducial marker locations and were along the Z axis. More notably, the deviations at the nasion were tightly clustered around a mean Z deviation of approximately 0.6 mm along the Z axis. In this case, the magnitude was approximately the discrete slice thickness of the CT scan (0.625 mm). It is plausible that this deviation results from a digital quantitization error in the process of generating the STL model from the MDCT scan data.

Quantization error results from constructing a model from discrete data (layers and pixels) contained in the MDCT scan data. The model is generated from discrete voxels, or 3-D digital blocks in space, as opposed to an infinitesimal point in space. The voxels generated from the conversion of the DICOM to a volumetric model of the control image is orthotropic with dimensions of 420 × 420 × 625 mm along the X,Y, Z directions, respectively. Standard deviations generally ranged from 30 to 80 mm, with one outlier at 230 mm. When compared to the voxel size, the standard deviations are less than the smallest voxel dimension. Errors in the RP model replication would most likely fall within the discrete resolution of the MDCT scan. The boundaries of the voxel are depicted in Figure 8 (as a bounding box); with the exception of a few outliers along Z, SLA model deviations from the control were within one voxel. In essence, the voxel size generated from the MDCT is larger than the deviations detected between any model and the control. The conversion of the DICOM data to STL files appears to be a limiting factor in the accuracy of the RP models in comparison to the control.

Results from the current study were consistent with the findings of other authors in that the SLA sample models were appropriate within a margin of error that is acceptable for clinical applications.[1,3,5] Furthermore, the method of measurement used in the current study was able to indicate which axis of fabrication would have the greatest deviation, and the magnitude of the deviation in relation to a voxel size.

CONCLUSIONS

The results of this study indicate that in a controlled setting, the greatest discrepancies of medical model fabrication correspond to the largest dimension of the orthotropic voxel volume of the MDCT scan, which is

related to the slice thickness of the scan and the Z axis of the RP model. Clinicians should be aware that the traditional imaging protocols for diagnosis that allow for large slice thickness, although they provide less exposure to the patient, may be less desirable for use in surgical manipulation software and accurate rapid prototype models and implants.

REFERENCES

1. Nizam A, Gopal R, Hakim A, Samsudin A. Dimensional accuracy of the skull models produced by rapid prototyping technology using stereolithography apparatus. Arch Orofac Sci 2006; 1:60-6.
2. Gronet PM, Waskewicz GA, Richardson. Preformed acrylic cranial implants using fused deposition modeling: a clinical report. J Prosthet Dent 2003; 90:429-33.
3. Galantucci L, Percoco G, Angelelli G, Lopez C, Introna F, Luizzi C, et al. Reverse engineering techniques applied to a human skull for CAD 3D reconstruction and physical replication by rapid prototyping. J Med Eng Tech 2006;30:102-11.
4. Furultan M, Fallahi B, Mottavalli S, Dujouvy M. Stereolithography: application to neurosurgery. Crit Rev Neurosurg 1998;20;8;203-8.
5. Winder J, Bibb R. Medical rapid prototyping technologies: state of the art and current limitations for application in oral and maxillofacial surgery. J Oral Maxillofac Surg 2005; 63:1006-15.
6. Hassfeld S, Mühling J. Computer assisted oral and maxillofacial surgery--a review and an assessment of technology. Int J Oral Maxillofac Surg 2001;30:2-13.
7. Frühwald J, Schicho, K, Figl M, Benesch T, Watzinger F. Accuracy of craniofacial measurements: computed tomography and three-dimensional computed tomography compared with stereolithographic models. J Cranio Surg 2008;19; 22-6.
8. Barker TM, Earwaker WJS, Lisle DA. Accuracy of stereolithographic models of human anatomy. Australas Radiol 1994;38:106-11.
9. Mischkowski, R, Reinhard P, Lutz R, Neugebauer J, Brochhagen H, Keeve E, et al. Geometric accuracy of a newly developed cone-beam device for maxillofacial imaging. Oral Surg Oral Med Oral Path Oral Rad Endo 2007;104: 551-9.
10. Jamali AA, Deuel C, Perreira A, Salgado CJ, Hunter J, Strong, EB. Linear and angular measurements of computer generated models: are they accurate, valid, and reliable? Computer Aided Surgery 2007;12:278-85.
11. Meadows James D. Geometric dimensioning and tolerancing: applications and techniques for use in design, manufacturing, and inspection. Danvers, Mass: CRC Press, LLC, 1995, p. 441.
12. DuBrul, EL; Sicher and DeBrul's oral anatomy, 8th edition. St Louis: Ishiyaku EuroAmerica, Inc; 1988. p. 61-65.

Corresponding author:
Dr Gerald Grant
Director, Craiofacial Imaging Research
Naval Postgraduate Dental School
8901 Wisconsin Avenue
Bethesda, MD 20889
Fax: 301-295-2119
E-mail: Gerald.grant@med.navy.mil

NOTEWORTHY ABSTRACTS OF THE CURRENT LITERATURE

Color related to ceramic and zirconia restorations: a review

Vichi A, Louca C, Corciolani G, Ferrari M.
Dent Mater. 2011;27:97-108.

The requirement to achieve natural looking restorations is one of the most challenging aspects of dentistry, and the shade matching of dental restorations with the natural dentition is a difficult task due to the complex optical characteristics of natural teeth. Dental porcelain is considered the reference material for prosthetic rehabilitation, but it is not easy to handle and aesthetic excellence is quite difficult to obtain. For these reasons, shade matching with dental porcelain is often considered to be more artistic than scientific. Shade matching is considered unpredictable due to several variables that may influence the final appearance of a restoration. In order to improve this situation, over the last decade new shade guides and instruments have been developed and the aesthetic aspects of dental porcelain have been further investigated. In this review some aspects of color selection and color reproduction have been examined. Color selection has advanced through the development of new shade guides and electronic shade taking devices, although visual assessment has still not been entirely replaced by electronic instruments. Color reproduction with dental porcelain has improved thanks to advances in the performance and knowledge of dental porcelain, but is still not easy to achieve. The difficulties of achieving good aesthetics with PFM restorations and the desire for metal free solutions have resulted in the increased use of zirconia. The unique optical properties of zirconia have introduced new opportunities for achieving superior aesthetics, however further research is required with this material.
Reprinted with permission of the Academy of Dental Materials.